LRG1 is a novel ligand of HER3 and promotes metastatic colorectal cancer growth

Moeez Rathore[1, 2], Michel'le Wright[1, 2], Wei Huang[3], Derek J. Taylor[3, 4], Yamu Li[2, 5] Zhenghe Wang[2, 5], Hao Feng[2, 6], Jordan Winter[1, 2, 7], Suneel Apte[8], Masaru Miyagi[3], John Greenwood[9], Stephen Moss[9], and Rui Wang[1, 2, 7 #]

1. Department of Surgery, Case Western Reserve University, 10900 Euclid Ave., Cleveland, OH 44106. USA

2. Case Comprehensive Cancer Center, Case Western Reserve University, 10900 Euclid Ave., Cleveland, OH 44106. USA

3. Department of Pharmacology, Case Western Reserve University, 10900 Euclid Ave., Cleveland, OH 44106. USA

4. Department of Biochemistry, Case Western Reserve University, 10900 Euclid Ave., Cleveland, OH 44106. USA

5. Department of Genetics and Genome Sciences, Case Western Reserve University, 10900 Euclid Ave., Cleveland, OH 44106. USA

6. Department of Population and Quantitative Health Sciences, Case Western Reserve University, Cleveland, OH, 44106, USA

7. Department of Surgery, Division of Surgical Oncology, University Hospitals Cleveland Medical Center, 11100 Euclid Avenue, Cleveland, OH 44106, USA

8. Department of Biomedical Engineering and Musculoskeletal Research Center, Cleveland Clinic Lerner Research Institute, Cleveland, OH 44106. USA

9. Institute of Ophthalmology, University College London, London, SE5 8BN, UK

Key words: LRG1, HER3, colorectal cancer, metastasis, liver endothelium, angiocrine.

 # Corresponding author:

Rui Wang, Ph.D.

Department of Surgery

Case Western Reserve University

10900 Euclid Ave. Wolstein Research Building Room 2127

Cleveland, OH 44106-7284, USA

Tel: 216-368-5667

Fax: 216-368-1166

Email: RXW517@case.edu

Conflict of Interest

The authors declare no potential conflicts of interest.

Abstract

Background: We previously reported that liver endothelial cells (ECs), a key component of the liver microenvironment, secrete soluble factors to promote CRC growth via activating human epidermal growth factor receptor (ErbB3, also known as HER3). However, we found that EC-induced HER3 activation is independent of the canonical HER3 ligand neuregulins (NRGs). The present study identified EC-secreted LRG1 as a new HER3 ligand for promoting CRC growth and elucidated the novel downstream signaling pathway induced by LRG1-HER3.

Methods: We first measured the binding affinity between HER3 and LRG1 by Biolayer interferometry (BLI). We then used in vitro and in vivo xenograft approaches to determine the effect of LRG1 monoclonal antibody (15C4) on HER3 activation and CRC growth. To further determine the role of LRG1 in promoting CRC growth in the liver, we used murine CRC cells in a syngeneic orthotropic liver injection model to establish CRC allografts in the liver of mice with systemic LRG1 knockout (LRG1-/-) and wild-type siblings (LRG1+/+). We also performed unbiased phospho-MS analysis and subsequent validations to determine the downstream signaling pathway activated by LRG1-HER3.

Results: We identified that LRG1 binds to HER3 with the affinity at ~100nM. The LRG1 antibody 15C4 completely attenuated LRG1-induced HER3 activation and in vitro and xenograft growth in vivo. Moreover, LRG1-/- mice with CRC allografts in the liver had significantly longer overall survival than tumor-bearing LRG1+/+ mice. Lastly, unbiased -omics analysis identified eIF4-protein synthesis is significantly activated by LRG1. With target-specific inhibitors, we further determined that LRG1-HER3 activates the PI3K-PDK1-RSK2-eIF4 axis independent of AKT.

Conclusions: We identified LRG1 as a novel HER3 ligand and demonstrated that the liver microenvironment-derived LRG1 plays a key oncogenic role in mCRC, by activating a novel RSK2-eIF4 survival pathway. Our findings highlighted the potential of blocking LRG1-HER3 and involved downstream pathways for treating patients with mCRC.

MATERIALS AND METHODS

Cell culture

Established human colorectal cancer (CRC) cell lines SW620 and HCT116 were purchased from American Type Culture Collection (ATCC, Manassas, VA). Murine CRC MC38 cells were kindly shared by Dr. Zhenghe Wang at Case Western Reserve University. The patient-derived CRC primary cell line HCP-1 was established, and kindly shared by, Dr. Lee Ellis from M.D. Anderson Cancer Center as described previously[1]. Primary human liver endothelial cells (EC-1, 3, 6, 9, and 11) were isolated and established using MACS microbead-conjugated antibodies (anti-EpCAM for HCP-1, and ant-CD31 for liver ECs) and separation columns, as described previously[1-6]. All CRC cells were cultured in MEM (Sigma-aldrich, St. Louis, MO) supplemented with 5% FBS (Atlanta Biologicals, Atlanta, GA), vitamins (1x), nonessential amino acids (1x), penicillin-streptomycin antibiotics (1x), sodium pyruvate (1x), and L-glutamine (1x), all from ThermoFisher/Gibco (Grand Island, NY). Primary liver ECs were cultured in Endothelial Cell Growth Medium MV2 (PromoCell, Heidelberg, Germany) supplemented with 10% human serum (Sigma) and antibiotics-antimycotic (1x, ThermoFisher/Gibco).

HCP-1 cells and liver ECs were used within 12 passages, with approximately ~1 week per massage. Mycoplasma contamination and short tandem repeat (STR) authentication tests for all cell lines are done every 6 months by the Genomics Core at Case Comprehensive Cancer Center, Case Western Reserve University. For primary cell lines (HCP-1 and liver ECs), genomic DNA samples from original patient tissues were used for STR authentication.

Animals

All experiments involving mice were approved by the Case Western Reserve University Institutional Animal Care Regulations and Use Committee (IACUC protocol # 2019-0087), and were done in 6-8 weeks old mice. Athymic nude mice and C57BL/6 mice were obtained from The Jackson Laboratory. Genetically engineered mouse model (GEMM) with systemic LRG1 knockout (LRG1 KO, C57BL/6N-*Lrg1*$^{tm1(KOMP)Vlcg}$/Mmucd)

were created and described before[7]. Heterogeneous mating pairs (*Lrg*$^{-/+}$) were purchased from Mutant Mouse Resource & Research Centers (Stock number 048463-UCD), and were used for making LRG1 knockout (*Lrg*$^{-/-}$) and wild-type siblings (WT). Genotyping was done using primers: SU: TCCTGGTGGGAGAGGACTC. SD: GACCCCTGAAACAGACGTG. LacZRev: GTCTGTCCTAGCTTCCTCACTG. NeoFwd: TCATTCTCAGTATTGTTTTGCC.

Reagents

The LRG1 monoclonal antibody 15C4 was developed in prior studies[8], and shared by Drs John Greenwood and Stephen E Moss at University College London, UK. Control human IgG antibody for *in vitro* and *in vivo* studies was from Invitrogen (Carlsbad, CA). Recombinant human LRG1 (Cat# 13371-HCCH), HER3 extracellular domain (HER3-ECD, Cat# 10201-H08H) and HER2 extracellular domain (HER2-ECD, Cat# 10004-H08H) were from Sinobiological (Houston, TX). Recombinant human NRG1 was from BioVision (Cat# 4711-10, Waltham, MA). Human *NRG1*-specific siRNAs (5'-UCGGCUGCAGGUUCCAAAC, and 5'-GGCCAGCUUCUACAAGCAU), *ERBB3* (HER3)-specific siRNAs (si-3: 5'-GCUGAGAACCAAUACCAGA, si-4: 5'-CCAAGGGCCCAAUCUACAA) and a validated scrambled control siRNA were obtained from Sigma-Aldrich (St. Louis, MO). Human siRNA smart pools for *LRG1* (Cat# sc-97202), *RPS6KA1* (RSK1, Cat# sc-29475), *RPS6KA2* (RSK2, Cat# sc-36443), and *RPS6KA3* (RSK3, Cat# sc-36441) were obtained from Santa Cruz Biotechnology. Human CRC tissue microarrays were obtained from US Biomax (Cat# CO246, Derwood, MD). Inhibitors for AKT (MK-2206, Cat. #S1078), RSK (BI-D1870, Cat. #S2843), PDK (BX-795, Cat. #S1274), PI3Kα (BYL719 Cat. #S2814), IRS1/2 (NT157 Cat. #S8228), eIF4E/4G (4EGI-1, Cat. #S7369) were obtained from Selleckchem (Houston, TX). Matrigel was from the R&D systems (Cat. # 3533-001-02. Minneapolis, MN).

Conditioned medium (CM)

$0.3x10^6$ CRC cells or ECs were seeded in T25 culture flasks overnight. Next day cells were washed two times with 1X PBS and then cultured in growth medium with 3ml 1% FBS ($0.1x10^6$ cells/ml) for 48 hours. CM was harvested and centrifuged at 2,000 *g* for 5 minutes to remove cell debris. CM from each CRC cell line were used as controls.

siRNA transfection

For each transfection, $1x10^6$ CRC cells were transiently transfected with 400 pmol siRNAs via electroporation by Neon Transfection System (Invitrogen, Carlsbad, CA) with 3 pulses of 10 msec at 1,600 V according to the manufacturer's instructions. Cells were recovered in 5% FBS for 24-48 hours, cultured in 1% FBS overnight, and then subjected to CM for 30 minutes for Western Blotting, or 72 hours for the MTT assay. Transfection of ECs with *LRG1* siRNAs was carried out using Lipofectamine RNAiMAX (Life Technologies, CA), at a final concentration of 50 nM. Unless stated otherwise, cells were recovered for three days after transfection before used.

LRG1 depletion from CM

ECs were transfected by control or *LRG1*-specific siRNAs and recovered for 72h. CM from transfected cells were then prepared as described before. For LRG1 immuno-depletion by antibodies, 5 µg control IgG or anti-LRG1 antibodies (both from R&D Systems) were added to 500 µl of 3X CM (1000 µg total proteins) from un-modified ECs After rocking overnight at 4°C, a 50 µl mixture of protein A/G PLUS-Agarose beads was added to CM and rocked at 4°C for 1 hour. CMs after immuno-depletion were used for treating CRC cells and tumors, or Western blotting. Beads with proteins were also used for Western blotting.

Size execution fractionation

5mL 10x concentrated CM from ECs and CRC were injected into the Superdex 200 increase 10/300 GL size exclusion chromatography column (Sigma Cat#GE28-9909-44). 200µl CM before column exclusion were saved as input for future analysis. After samples were loaded into the column, the first elution was performed with 5% of Hepes buffer (20mM Hepes, pH 7.5, 1M NaCl) for 5mL to remove weakly bound proteins. 20 fractions were collected with 0.5 mL/fraction. All fractions were stored at 4°C and used within 3 days, either for CRC cell treatments, Western blotting, or for mass spectrometry (MS).

Pull-down Assay with HER3-ECD

2 µg purified HER3-ECD or control HER2-ECD (both have His-tag fused at the C-terminal) were added to 500 µl of 10X concentrated EC CM and incubated overnight at 4°C and with gentle rocking. Next day, 50 µl Ni-NTA beads were added to the mixture and incubated for 1 h at 4°C with gentle rocking, and then centrifuged at 13,000 *g* for 2 minutes. After removing the supernatant, Ni-NTA beads were wash twice with 0.5 ml 20mM imidazole, and then incubated in 50 µl of 500 mM imidazole for 5 minutes at room temperature, and centrifuged at 13,000 *g* for 2 minutes. Supernatant with eluted soluble proteins were used either for treating CRC cells, Western blotting, or for MS analysis. Ni-NTA beads were also used for Western blotting.

Mass spectrometry (MS)

MS analysis for fractionated CM or for pulled-down proteins by HER3- or HER2-CD were all done at Taplin Mass spectrometry Facility, Harvard Medical School, Boston, MA. Samples were treated with trypsin overnight at 37°C and acidified by spiking in 20ul 20% formic acid solution and then desalted by STAGE tip. Samples were then reconstituted in 10 µl HPLC solvent A. After equilibrating the column, each sample was

loaded via a Famos auto sampler (LC Packings, San Francisco CA) onto the column. A gradient was formed and peptides were eluted with increasing concentrations of solvent B (97.5% acetonitrile, 0.1% formic acid). Eluted peptides were subjected to electrospray ionization and then entered into an LTQ Orbitrap Velos Elite ion-trap mass spectrometer (Thermo Fisher Scientific, Waltham, MA). Peptides were detected, isolated, and fragmented to produce a tandem mass spectrum of specific fragment ions for each peptide. Peptide sequences (and hence protein identity) were determined by matching protein databases with the acquired fragmentation pattern by the software program, Sequest (Thermo Fisher Scientific, Waltham, MA).

Western blotting

CRC cells were treated with CM, antibodies, or specific inhibitors for 30 minutes. Cell lysates were processed and run through SDS-PAGE gel electrophoresis as described previously[1-5]. For CM samples and or bead-bound proteins in pull-down assays, CM and beads were boiled with SDS-PAGE buffer for 5 minutes. HRP conjugated β-actin antibody was from Santa Cruz Biotechnology, and LRG1 antibody was from R&D Systems (Cat# AF78900). All other antibodies were from Cell Signaling (Beverly, MA). For each experiment, protein samples were loaded to two gels and processed at the same time for separately probing for antibodies specific to phosphorylated proteins and total proteins, and for detecting proteins that have similar sizes. All membranes were probed with β-actin as loading control and a representative image was shown for each experiment. Each Western Blotting figure shows representative results of at least three independent experiments.

Phospho-proteomics analysis

HCP-1 CRC cells were seeded at 5 x 10^6 cells/well in 10cm plates, cultured in 1% FBS overnight and then treated with EC CM for 30min, with HCP-1 CM as controls. Cells were then washed twice with cold 1X PBS and cell pellets were harvested following trypsin treatment and centrifugation. Cell pellets from three independent experiment

were sent to the Proteomic and Metabolomics core at Lerner Research institute, Cleveland clinic, Cleveland, OH, for global serine (S) and threonine (T) phosphorylation analysis. Cell pellets digested with trypsin and then subjected to phospho-S/T enrichment using Fe-NTA spin columns from ThermoScientific. The enriched samples were analyzed by LC-MS/MS by a ThermoScientific Fusion Lumos mass spectrometry system and the goal of these experiments is to quantify the relative abundance of the phospho-S/T peptides.

Identification and quantification of phosphor-peptides were done with Andromeda search engine integrated into the MaxQuant version 1.6.3.3 against UniProt human proteome database. Principal component analysis and volcano plot (FDR = 0.01, S0=0.1) were used for sample clustering, and QIAGEN Ingenuity Pathway Analysis (QIAGEN IPA) was used for pathway and functional analyses of identified significantly and differentially phosphorylated proteins in HCP-1 cells treated by control HCP-1 CM or EC CM.

MTT assay

CRC cells were seeded at 3,000 cells/well in 96-well plates, cultured in 1% FBS overnight and then treated with CM for 72 hours. When the LRG1 antibody 15C4 (500 µg/ml) was used, cells were pretreated with 15C4 in 1% FBS medium for 6 hours, and then cultured in CM with or without 15C4 for 72 hours. Cell viability was assessed by adding MTT substrate (0.25% in PBS, Sigma) in growth medium (1:5 dilution) for 1 hour at 37 °C. Cells were washed with 1x PBS and then incubated in 50 µl DMSO. Optical density was measured at 570 nm and relative MTT was presented as % of control.

Global Protein Synthesis

The Global protein synthesis assay kit from Abcam (Cat# ab273286, Waltham, MA) was used following to the manufacturer's instructions. In brief, CRC cells were seeded 100,000 cells/well in 96-well plates, cultured in 1% FBS overnight and then incubated

with CM and O-Propargyl-puromycin (OP-puro) analogs for *de novo* protein labeling for 24 hr. Next, day, cells were fixed, permeabilized, labeled with florescence probes. Cells were also labeled with DAPI for total loading controls. Intensities of florescence probes and DAPI were measured by an EVOS cell imaging system (Invitrogen), and presented as % of control relative to DAPI.

Subcutaneous (subQ) xenograft model

$1x10^6$ HCP-1 or $2x10^6$ SW620 cells were injected subQ into the right flanks of athymic nude mice in 100 µL growth-factor-reduced Matrigel. After xenografts were confirmed, mice were randomized and then treated with 3x concentrated CRC or EC CM once a week by injecting CM subQ into the spaces between xenografts and skin tissues. Tumor volumes were measured with a caliper. All mice were euthanized when 3 mice from any group became moribund or tumor sizes reach $2000mm^3$, and tumor tissues were harvested. For 15C4 treatments, mice were treated with CM and with either IgG control antibody or 15C4 30 mg/kg twice a week by intraperitoneal (IP) injection.

Orthotropic liver injection allograft model

For orthotropic allografts in the liver, luciferase reporter-labeled murine CRC cells (MC38) were suspended in an inoculation matrix (1:1 mix of growth-factor-reduced Matrigel and 1x PBS) and injected ($1x10^5$ cells in 30 µl/injection) into the left lobe of the liver of C57BL/6J mice. After injection, tumor burden was assessed by bioluminescence with the *In Vivo* Imaging System (IVIS) and D-Luciferin substrate (Xenogen, Alameda, CA) according to the manufacturer's instructions. For studies in GEMM with LRG1 knockout, MC38 cells were injected into mice with systemic knockout of LRG1 and wild-type siblings and tumor burden was monitored by IVIS. For studies with 15C4 treatments, wild-type C57BL/6 mice were purchased and used. Allograft burden was confirmed by IVIS and mice were randomized and then treated with control IgG or 15C4 antibodies (30 mg/kg by IP twice a week). Mice were sacrificed when became moribund. Tumor-bearing liver tissues were collected for analysis.

Immunohistochemistry (IHC)

Tumor tissues were fixed in 4% paraformaldehyde, dehydrated in ethanol, and embedded in paraffin. Sections were cut 10 μm in thickness. Human CRC tissue microarrays in 10 μm were purchased and used. IHC staining was done with antibodies against P-eIF4B S422 (1:200; Cell Signaling Technology, Cat# 3591), P-HER3 Y1289 (1:100; Cell Signaling Technology, Cat# 2842), and Ki-67 (1:200, Cell Signaling Technology, Cat# 9449T). Isotype-matched immunoglobulin was used as a control. The HRP-conjugated anti-rabbit secondary antibody (Cell Signaling Technology, Cat# 8114p) were used with the DAB substrate kit (Vector Laboratories, Newark, CA, SK-4800) for staining. Stained sections were examined under a light microscope (Olympus BX51). Intensity of the staining was quantified by QuPath software (NIH) and presented as density relative to control groups with CRC CM.

Statistical analysis

For *in vitro* assays, all quantitative data were reproduced in at least three independent experiments with multiple measures in each replicate. Groups were compared by unpaired two-tailed Student's *t*-test and data was expressed as means -/+ standard error of the mean (SEM.) with significance of $P<0.05$. For *in vivo* assays, Wilcoxon rank-sum test was used for tumor volume and burden change over time, and for Kaplan-Meier plots for overall survival. One-way ANOVA was used for comparing between-group difference analysis after collecting tissues at the end of experiments, and IHC analysis with human tissues. *In vivo* data was expressed as means -/+ standard deviation (SD) with significance of $P<0.05$.

INTRODUCTION

Patients with primary and localized colorectal cancer (CRC) have 5-year survival rates between 53%-92% and are potentially curable by surgical resection and adjuvant therapy when appropriate [9]. However, patients with metastatic CRC (mCRC) only have a 5-year survival rate at 14% [9]. Therapy failure for patients with mCRC remains an overarching challenge in the clinic.

Over 80% of CRC metastases occur in the liver [10], which has a unique endothelial cell (EC)-rich microenvironment, with up to ~40% of liver stroma composed of endothelial cells (ECs) [11-13]. Preclinical studies used established EC lines, most with human umbilical vein endothelial cells, and showed that as a critical component of the microenvironment, endothelial cells (ECs) promote cancer cell survival pathways by secreting soluble factors in a paracrine fashion, named angiocrine, in different types of cancer [14-17]. The pathophysiological paracrine roles of ECs in CRC were first demonstrated in a prior study showing that EC-secreted Jagged-1 activated the cancer stem cell-associated pathway Notch for promoting cancer stem cell phenotypes in CRC [1]. Distinct from most preclinical studies in angiocrine signaling, this study established a strategy for isolating and culturing primary ECs from human liver tissues. These findings not only suggest the distinct EC microenvironment in the liver may promote survival in CRC liver metastases, the latter study in CRC also developed a novel preclinical model for studying specific angiocrine roles of liver ECs. Following the logic, we used primary liver ECs derived from surgically resected non-neoplastic liver tissues, and determined that liver ECs secreted soluble factors in conditioned medium (CM) that, in turn, activated human epidermal growth factor receptor 3 (HER3, also known as ErbB3) for promoting CRC cell survival [2,6]. Interestingly, we found that the only identified HER3 ligand to date, neuregulins (NRGs), are not involved in liver EC-induced HER3 activation in CRC cells, suggesting liver ECs secrete a novel HER3 ligand that has not been identified. As we recently determined for the first time that HER3 phosphorylation activation is associated with mCRC progression, with higher levels in mCRC liver metastases than in primary tumors or lymph metastases, (**Suppl. Fig. 1**), identifying the

novel HER3 ligand secreted by ECs will help us to further elucidate the pro-tumor roles of liver ECs in mCRC development.

In the present study, we conducted unbiased proteomics analysis and identified leucine-rich alpha-2-glycoprotein 1 (LRG1) as a novel HER3 ligand that was secreted by liver ECs for promoting CRC cell functions. We demonstrated that depleting LRG1 from EC CM or neutralizing secreted LRG1 with an antibody completely blocked EC-induced HER3 activation and CRC cell survival. Moreover, we used orthotopic mCRC models and determined that LRG1 perturbations, either by LRG1 systemic knockout (LRG1 KO) or a LRG1 neutralizing antibody, significantly decreased mCRC tumor growth in the liver and prolonged mice overall survival. Lastly, we elucidated that LRG1 activated HER3 and the downstream PI3K-PDK-RSK-eIF4 axis, distinct from NRGs, and promoted eIF4-mediated protein synthesis in CRC cells. As developed HER3-specific inhibitors and antibodies had limited impact in the clinic[18], with the exception in patients with rare *NRG1* fusion mutations [19-22], our findings highlight a potential strategy of blocking LRG1, and potentially other specific components in the LRG1-HER3 signaling cascade, for treating patients with mCRC.

RESULTS

EC-secreted LRG1 is a new ligand for HER3 activation

As primary ECs were derived from patients with distinct pathophysiological conditions, we used five distinct primary liver EC lines derived from different patients and further confirmed the angiocrine role of ECs in promoting CRC cell growth, determined by the MTT assay, in a PDX-derived CRC cell line HCP-1 and two established CRC cell lines (SW620 and HCT116. **Suppl. Fig. 2A**). We also validated that depleting the only known HER3 ligand NRGs from EC CM did not affect EC-induced HER3 activation in CRC cells (**Suppl. Fig. 2B**). Of note, *NRG2* that also encodes for NRG proteins is not expressed in ECs or cancer cells[23,24]. To identify the novel EC-secreted soluble factor(s) that activate CRC-associated HER3, we first fractionated EC CM by fast protein liquid chromatography and found that soluble factors in fractions 7 and 8 activated HER3 in

CRC cells, as determined by Western blotting for HER3 phosphorylation with lysates from CRC cells treated by fractions (**Fig. 1A, B**). We then sent the remaining fractions 7 and 8 for protein identification by mass spectrometry (MS #1). Separately, we used a purified human HER3 extracellular domain (HER3-ECD) peptide to pull down HER3-activating factor(s) from EC CM. As a result, EC CM after HER3-ECD pull-down could not activate HER3, whereas the soluble factor(s) pulled down and eluted from HER3-ECD activated HER3 when incubated with CRC cells. In parallel, empty Ni-NTA beads and purified HER2-ECD were used as negative controls, and they did not pull down HER3-activating factor(s) from EC CM (**Fig. 1C, D**). As a result, EC CM depleted by HER3-ECD failed to promote growth, compared to complete EC CM or EC CM depleted by controls (**Fig. 1E**). Similar effects of HER3-ECD depleting HER3-activating factor(s) from EC CM were also observed when using CM from other EC lines with additional CRC cells (**Suppl. Fig. 3A**). Subsequently, soluble factors eluted from Ni-NTA beads, HER2-ECD, or HER3-ECD were sent for MS analysis (MS #2). In both MS analyses, CM of HCP-1 CRC cells were processed and analyzed in parallel as negative controls. By comparing data from MS #1 and MS #2, we identified the top 10 candidate secreted soluble proteins that were exclusively found in EC CM fractions that activated HER3 (MS #1) and bound to HER3 (MS #2) (**Suppl. Fig. 3B**, **Table 1,** ranked by abundance). To identify the specific protein that activates HER3, we treated CRC cells with human recombinant form of each candidate protein and found that only LRG1 activated HER3 and promote CRC cell growth (**Fig. 1F, G),** whereas other candidate proteins did not activate CRC-associated HER3. Next, we confirmed that LRG1 was detected in EC CM and was pulled down by HER3-ECD (**Fig. 1H, I**). We then performed the surface plasmon resonance (SPR) assay and determined the binding affinity of LRG1 for HER3 is at K_D=100 nM (**Fig. 1J**). Together these findings determined that LRG1 directly binds to and activate HER3 in CRC cells for mediating EC-induced CRC functions.

LRG1 activates HER3 to promote CRC growth

LRG1 is known to be secreted by ECs, and a few other types of cells, to activate TGFβ receptors and downstream SMAD signaling for promoting cell growth and migration[25,26]. However, significant CRC cells harbor loss-of-function mutations in TGFβ receptor

genes(published data[27,28], and CCLE database). As a result, LRG1 could not activate SMAD family proteins in CRC cells with TGFβ receptor mutations. Moreover, we found that even in CRC cells with function TGFβ receptors (SW620 and HT29), LRG1 activated HER3 without affecting SMAD proteins, whereas TGFβ activated SMAD3, as expected, but had no effect on HER3 (**Suppl. Fig. 3B**). Together these findings further confirmed that LRG1 activates HER3, moreover, we determined that LRG1-HER3 interaction is independent of TGFβ receptors.

To further determine roles of EC-secreted LRG1 in HER3 activation and CRC cell functions, we first depleted LRG1 from EC CM by transfecting ECs with LRG1-specific siRNAs to knock down LRG1 expression, with scramble siRNAs as a control (**Fig. 2A**). We then treated CRC cells with CM from ECs either with control siRNAs or with LRG1-specific siRNAs, and determined that CM with LRG1 activated HER3 and increased CRC cell growth, as expected, whereas depleting LRG1 from EC CM by siRNA knockdown completely abolished EC-induced HER3 activation and cell growth (**Fig. 2B, C**). As an additional validation, we immune-depleted soluble LRG1 from EC CM with a commercially available LRG1 antibody and showed that immune-depletion of LRG1 also completely blocked HER3 activation and elevated cell growth caused by EC CM (**Fig. 2D—F**). To determine the effects of liver EC-secreted LRG1 on CRC growth *in vivo*, we used a proof-of-principle xenograft model with CRC cells, as done before [2,5,6]. First, we subcutaneously (subQ) implanted CRC cells into athymic nude mice. Once xenografts were established, mice were randomized with equal tumor size and then treated with CM by subQ injecting CM into the spaces between xenografts and skin tissues once a week. Compared to control CM from CRC cells themselves, complete EC CM led to significant 3-5-fold increases in tumor sizes in both cell lines, as expected. More importantly, immuno-depleting LRG1 from EC CM completely abolished EC-induced xenograft growth (**Fig. 2G**). Together, these findings from *in vitro* and *in vivo* studies demonstrated that LRG1 is the key mediator of EC-induced HER3 activation and CRC growth.

LRG1 blockade reduced tumor growth and increases mice overall survival in orthotopic mCRC models

To better recapitulate the effects of liver ECs and LRG1 on CRC liver metastases, we used a liver injection orthotopic xenograft model to establish mCRC in the liver of LRG1 KO mice with wild-type siblings (WT). After genotyping and LRG1 expression confirmed, as done before[7], luciferase-labeled MC-38 murine CRC cells were implanted into the left lobes of livers for developing orthotopic mCRC allografts. Compared to WT mice, LRG1 KO mice had significantly slower mCRC tumor growth, resulting in longer overall survival (50 days in WT mice, 80 days in LRG1 KO mice. **Fig. 3A**).

Subsequently, we further determined the effects of LRG1 blockade on mCRC tumor growth with a LRG1 neutralizing antibody, 15C4, that was developed to specifically bind and neutralize human and murine LRG1 *in vivo*, and demonstrated strong on-target effects in other disease models [29-31]. We first showed that 15C4 blocked EC-induced HER3 activation and growth in CRC cells (**Fig. 3B, C**). Then, we established subQ xenografts with HCP-1 cells in athymic nude mice. After xenografts were established, we treated xenografts with CRC or EC CM, and I.P. injected 15C4 into tumor bearing mice twice a week. While EC CM significantly increased tumor growth, as expected, 15C4 completely blocked EC-induced tumor growth (**Fig. 3D**). Paired with that, the levels of HER3 phosphorylation, indication of activation, in xenografts were increased by EC CM, and blocked by 15C4 (**Fig. 3E**). Interestingly, 15C4 had little effect on CRC cells or subQ xenografts without EC CM treatment, suggesting LRG1 blockade may have limited effect on CRC primary tumors without the rich EC-microenvironment in the liver. Indeed, a prior study used LRG1 KO mice and showed that LRG1 depletion only modestly decreased intestinal polys developed in *Apc*$^{min/+}$ and villin-Cre, *Apc*$^{flox/+}$ models. Our findings, together with others, suggest that EC-secreted LRG1 plays a critical role in promoting mCRC growth in the liver.

eIF4-protein synthesis is a novel downstream pathway of the LRG1-HER3 axis

To determine the downstream pathway(s) that mediate LRG1-HER3 induced CRC functions, we compared the protein phosphorylation landscapes between CRC CM- or EC CM-treated CRC cells by the phospho-serine/threonine enrichment LC/MS analysis. Principal component analysis determined that the determined protein phosphorylation landscapes between CRC and EC CM treated groups are significantly different, with 75.2% and 11.7% variances (**Fig. 4A**), and 497 identified significant between-group differences (**Fig. 4B**). We then conducted QIAGEN Ingenuity Pathway Analysis (IPA) for pathway and functional analyses with the identified 497 significant changes and found protein synthesis and eIF4 as the top EC-activated cell function and pathway, respectively (**Table 2**). As eIF4 is a major signaling pathway for regulating eucaryotic cell protein synthesis[32], the data strongly suggest that LRG1-HER3 activates eIF4-protein synthesis in CRC cells, which has not been reported before in LRG1 or HER3 signaling studies. To validate our findings and determine the role of LRG1-HER3 in activating eIF4 protein synthesis, we first confirmed that LRG1 increased eIF4B phosphorylation, a key readout of eIF4 complex activation in CRC cells, and then determined that HER3 siRNA knockdown completely blocked LRG1-induced eIF4B phosphorylation (**Fig. 4C**). Coupled with that, the LRG1 neutralizing antibody 15C4 blocked EC-induced eIF4B phosphorylation and *de novo* protein synthesis in CRC cells (**Fig. 4D, E**), and that an eIF4 inhibitor completely blocked EC-induced CRC growth (**Fig. 4F**). Lastly, as it is challenging to assess *de novo* protein synthesis *in vivo*, we analyzed the CRC xenografts treated by EC CM and 15C4 in **Fig. 3D**, and found that the levels of eIF4B phosphorylation was increased by EC CM and decreased by 15C4 (**Fig. 4G**). These findings identify eIF4-mediated protein synthesis as a novel downstream target of the LRG1-HER3 axis.

The PI3K-PDK1-RSK axis mediates LRG1-induced eIF4 activation and protein synthesis

To elucidate the mechanism by which LRG1-HER3 activates eIF4, we compared the effects of LRG1 and the established HER3 ligand neuregulins on CRC cells and found that eIF4 was specifically activated by LRG1, not neuregulins (**Fig. 5A**). IPA identified

AKT-mTOR as another top EC-activated pathway (**Table 2**), which is a major upstream effector of eIF4[33], and can be activated by canonical NRG-activated HER3[18]. Interestingly, we found that NRG1 treatment activated AKT, as expected, but LRG1 had no effect on AKT. As an allosteric AKT inhibitor MK-2206 and found that it did not block LRG1-induced eIF4B activation (**Fig. 5B**), our data suggest that the LRG1-HER3 axis induced eIF4B independent of the established AKT signaling. Prior studies reported separately that RSK2 is another upstream effector of eIF4[33,34], and that RSK2 can be activated by the PI3K-PDK1 axis independent of AKT[35,36]. Therefore, it is possible that the PI3K-PDK1-RSK2 axis is a novel downstream target of LRG1-HER3 and mediates eIF4 activation independent of AKT. To test this hypothesis, we used specific inhibitors separately to block PI3K (by BYL719, a p110α inhibitor), PDK1 (by BX795), or RSK2 (by BI-D1870, a pan-RSK inhibitor) and found that indeed inhibiting each component of the axis blocked LRG1-induced eIF4B activation, protein synthesis, and growth in CRC cells (**Fig. 5C, D**, and **Suppl. Fig. 4A**). Of note, as IRS is a key mediator for RTK activation of PI3K in CRC cells[37,38], an IRS inhibitor (NT157) also blocked LRG1-induced eIF4B activation. In addition, inhibitors of p110β (TGX-221), another isoform of PI3K expressed in CRC cells, blocked eIF4B activation and protein synthesis (**Suppl. Fig. 4B, C**), suggesting p110β is also involved in LRG1-induced CRC cell functions. Together, our findings demonstrated a novel model of LRG1 inducing eIF4-mediated protein synthesis and growth via activating a novel PI3K-PDK1-RSK2-eIF4 axis, independent of the AKT-mTOR signaling (**Fig. 5E**).

DISCUSSION

Prior studies showed that ECs, as a critical component of the microenvironment, promote cancer cell survival by secreting soluble factors in a paracrine fashion in different cancer types[14-17]. Our laboratory uses primary liver ECs to recapitulate the liver EC microenvironment, and showed that liver EC-secreted factors promote CRC cell growth by activating CRC-associated HER3[2,6]. As, we found that ECs activate HER3 independent of the only known HER3 ligand, neuregulins, the present studies identified EC-secreted LRG1 as a novel HER3 ligand that

promotes CRC tumorigenesis, and determined the PI3K—eIF4 mediated protein synthesis as a novel downstream target of HER3 signaling.

LRG1 is secreted by ECs, and a few other cell types, and is known for activating the TGFβ receptor-SMAD axis to promote cell growth and migration[25,26]. However, role of LRG1 in CRC is unclear. CRC often harbor loss-of-function mutations in TGFβ receptors[27,28], and we found that LRG1 does not activate TGFβ receptor-SMAD in CRC. On the other hand, systemic LRG1 knockout decreased intestinal polyps in an *Apc*$^{Min/+}$ model, but the mechanism was unknown[31]. We found that liver EC-secreted LRG1 increased CRC tumor growth in proof-of-principle subcutaneous (subQ) xenograft models, and systemic LRG1 knockout prolonged mouse survival in an orthotopic mCRC model. Our findings determined a critical role of EC-secreted LRG1 in promoting mCRC development.

Our data, together with others[39], show that LRG1 is only secreted by ECs but not CRC cells. In contrast, limited studies from one group used different LRG1 antibodies and detected LRG1 protein levels in CRC cells and tissues[40-42]. However, they showed that LRG1 gene knockdown had little effect on CRC cell functions and their antibodies failed to detect decreased LRG1 by siRNAs, suggesting LRG1 was not expressed in CRC cells and the antibody they used was not specific for LRG1 detection. Meanwhile, detecting secreted soluble LRG1 in tissue sections remain a major challenge. LRG1 antibodies we use from R&D Systems were sufficient for Western blotting but not for IHC or IF staining, especially for soluble LRG1 in the interstitial space. Other studies used antibodies from other vendors and showed IHC staining of intracellular LRG1 (published data[40-42], and Human Protein Atlas). However, most prior IHC analyses did not include controls and had inconsistent patterns of LRG1 staining, suggesting non-specific staining. The specific expression of LRG1 in CRC and other types of cancer remain unclear and will be determined by future studies.

Taken together, the present studies determined a novel role of liver EC-secreted LRG1 in promoting CRC tumorigenesis after cancer cells metastasize to the liver, and will elucidate the mechanisms of LRG1 binding and activating HER3 as a newly identified ligand. Our findings highlight the oncogenic roles of the LRG1-HER3 axis in metastatic CRC progression and development, and identified HER3 phosphorylation as a potential prognostic biomarker for patients with metastatic CRC. Lastly, as LRG1-HER3 axis is distinct from the canonical

neuregulin-HER3 signaling, our data suggest potential novel therapeutic strategies for targeting LRG1 and other amenable component(s) in the LRG1-HER3 signaling cascade that are not addressed by the established HER3-targeted therapies.

FIGURE LEGENDS

Figure 1. LRG1 bound and activated HER3 as a novel ligand. (A) Schematics of CM fractionation by FPLC. **(B)** Western blotting showed P-HER3 levels in CRC cells after 30 minutes treating with EC-9 CM fractions. **(C)** Schematics of HER3-ECD with His tags pulling down soluble factors from EC-9 CM. Green, HER3-ECD. Red, EC-secreted factor(s) that bind to HER3-ECD. **(D)** Western blotting showed P-HER3 levels in CRC cells after 30 minutes treating with EC-9 CM after beads or ECD depletion, or with soluble factors eluted from beads or ECD. Ctrl beads: Ni-NAT beads only without ECD. Ctrl ECD: HER2-ECD. **(E)** The MTT assay showed CRC cell viability after 72 hours incubating with CM. **(F)** Western blotting showed P-HER3 levels in CRC cells after 30 minutes treating with LRG1 peptides. **(G)** The MTT assay showed CRC cell viability after 72 hours treating with CM or LRG1 (250 ng/ml). **(H)** Western blotting showed soluble LRG1 in CM from EC-1 and -9 cells. **(I)** Western blotting showed LRG1 pulled down by HER3-ECD. **(J)** SPR assay determined LRG1 and HER3-ECD binding affinity. $K_D=K_{on}/K_{off}$, 1:1 fit model. In (E) and (G), data are shown as Mean +/- SEM, ***$p<0.001$, **$p<0.01$, *$p<0.05$ by unpaired two-tailed *t*-test.

Figure 2. Depleting LRG1 from EC CM abolished EC-induced HER3 activation and growth in CRC cells and xenografts. (A) Western blotting showed LRG1 levels in CM from ECs with control or LRG1-specific siRNAs. **(B)** Western blotting showed P-HER3 levels in CRC cells after 30 minutes treating with CM from CRC, or from EC-9 with control or LRG1-specific siRNAs. **(C)** The MTT assay showed CRC cell viability after 72 hours incubating with CM. **(D)** Western blotting showed LRG1 levels on pull-down beads with control or LRG1 antibodies, or in EC-9 CM after immuno-depletion by control or LRG1 antibodies. **(E)** Western blotting showed P-HER3 levels in CRC cells after 30 minutes treating with CRC CM or EC-9 CM after immuno-depletion by control or LRG1 antibodies. **(F)** The MTT assay showed CRC cell viability after 72 hours incubating with CM. **(G)** Tumor volumes of subQ xenografts treated by CRC CM, complete EC-9 CM, or LRG1-depleted EC-9 CM (n=8 mice/group). For (C) and (F), data are shown as Mean

+/- SEM, **p<0.01, *p<0.05 by unpaired two-tailed *t*-test. For (G), data are Mean -/+ SD, **p<0.01, *p<0.05 by Wilcoxon rank-sum test.

Figure 3. Host LRG1 inhibition by gene knockout or antibodies blocked mCRC tumor growth in syngeneic, orthotopic models. (A) Kaplan-Meier curve for overall survival of mice with MC-38 mCRC allografts in the liver of WT mice and LRG1 KO mice (n=5 mice/group). **(B)** Western blotting showed P-HER3 levels in CRC cells after 30 minutes treating with CM and the LRG1 neutralizing antibody 15C4. **(C)** The MTT assay showed CRC cell viability after 72 hours incubating with CM and 15C4. **(D)** HCP-1 subQ xenograft mean volume over time, and images and weights of harvested subQ xenograft from mice treated with CM and 15C4 (n=10 mice/group). **(E)** Representative images of P-HER3 (Y1289) IHC staining of HCP-1 xenografts. For (A) and (D), data are Mean -/+ SD, **p<0.01, *p<0.05 by Wilcoxon rank-sum test. For (C), data are shown as Mean +/- SEM, ***p<0.001, **p<0.01, *p<0.05 by unpaired two-tailed *t*-test.

Figure 4. eIF4 protein synthesis is a novel downstream target of the LRG1-HER3 axis in CRC cells. (A, B) Principal component analysis and volcano plot were used for clustering of identified serine- and threonine-protein phosphorylation in CRC cells after 30 minutes culturing in CRC or EC-9 CM. **(C)** Western blotting showed P-eIF4B levels in CRC cells with or without siRNA of HER3 and after 30 minutes treating with or without LRG1. **(D)** Western blotting showed P-eIF4B levels in CRC cells after 30 minutes treating with CM and with or without the LRG1 neutralizing antibody 15C4. **(E)** The global protein synthesis assay showed the levels of *de novo* protein synthesis in CRC cells after 24 hours incubation with CM and 15C4. **(F)** The MTT assay showed CRC cell viability after 72 hours incubating with CM and an eIF4 inhibitor. **(G)** Representative images and quantifications of P-eIF4 IHC staining of HCP-1 xenografts treated by CM from CRC or EC-9, and with/without 15C4. For (E) and (F), data are shown as Mean +/- SEM, ***p<0.001, **p<0.01, *p<0.05.

Figure 5. The PI3K-PDK1-RSK2 axis mediates LRG1-induced eIF4 protein synthesis in CRC cells. (A) Western blotting showed P-HER3, P-eIF4B, and P-AKT levels in CRC cells after 30 minutes treating with either LRG1 or neuregulins (NRGs). **(B)** Western blotting showed P-eIF4B levels in CRC cells after 30 minutes treating with LRG1 and different doses of AKT inhibitors (MK-2206). **(C)** Western blotting showed P-eIF4B levels in CRC cells after 30 minutes treating with LRG1 and different doses of IRS inhibitors (NT157), p110α inhibitors (BYL719), PDK1 inhibitors (BX795), and RSK inhibitors (BI-D1870). **(D)** The global protein synthesis assay showed the levels of *de novo* protein synthesis in CRC cells after 24 hours incubation with LRG1 and specific inhibitors. **(E)** Schematics of the signaling pathway. For (D), data are shown as Mean +/- SEM, **p<0.01, by unpaired two-tailed *t*-test.

Supplementary Figure 1. Human mCRC liver metastases had higher levels of HER3 phosphorylation than normal or CRC at earlier stages. Representative images and quantifications of IHC staining of phospho-HER3 (P-HER3) at Y1289 using human tissues form normal mucosa, primary CRC, mCRC lymph node metastases, and mCRC liver metastases. Sections were counter stained with hematoxylin. Scale bars 100 µm. Mean +/- SD, *p<0.05 by one-way ANOVA test.

Supplementary Figure 2. CM form primary liver ECs increased CRC cell growth and HER3 activation independent of NRGs. (A) The MTT assay showed CRC cell viability after 72 hours incubation in CM from CRC cells or different liver EC lines. Mean +/- SEM, ***p<0.001, **p<0.01 by unpaired two-tailed *t*-test. **(B)** Western blotting showed NRG1 in CM from EC-9 cells with either control or NRG1-specific siRNAs, and P-HER3 levels in CRC cells after 30 minutes treating with CRC CM, or CM from EC-9 with control or NRG1-specific siRNAs.

Supplementary Figure 3. HER3-ECD bound to HER3-activating soluble factors and LRG1 did not activate TGFβ receptors in CRC cells, related to Figure 1. (A)

Western blotting showed P-HER3 levels in CRC cells after 30 minutes treating with EC-1 CM with or without beads or ECD depletion, or with soluble factors eluted from beads or ECD. **(B)** Western blotting showed P-HER3 and P-SMAD3 levels in CRC cells with functional TGFβ receptors after 30 minutes treating with LRG1 or TGFβ peptides.

Supplementary Figure 4. Additional validation of roles of the PI3K-PDK1-RSK2 axis in mediating LRG1-induced eIF4 protein synthesis. (A) Western blotting showed P-eIF4B levels in HCT116 cells after 30 minutes treating with LRG1 and different doses of IRS inhibitors (NT157), p110α inhibitors (BYL719), PDK1 inhibitors (BX795), and RSK inhibitors (BI-D1870). **(B)** Western blotting showed P-HER3 and P-eIF4B levels in CRC cells after 30 minutes treating with LRG1 and different doses of p110β inhibitors (TGX-221). **(C)** The global protein synthesis assay showed the levels of *de novo* protein synthesis in CRC cells after 24 hours incubation with LRG1 and p110β inhibitors, mean +/- SEM, **$p<0.01$, by unpaired two-tailed *t*-test.

REFERENCE

1. Lu, J., Ye, X., Fan, F., Xia, L., Bhattacharya, R., Bellister, S., Tozzi, F., Sceusi, E., Zhou, Y., Tachibana, I., et al. (2013). Endothelial cells promote the colorectal cancer stem cell phenotype through a soluble form of Jagged-1. Cancer Cell *23*, 171-185. 10.1016/j.ccr.2012.12.021.
2. Wang, R., Bhattacharya, R., Ye, X., Fan, F., Boulbes, D.R., and Ellis, L.M. (2019). Endothelial Cells Promote Colorectal Cancer Cell Survival by Activating the HER3-AKT Pathway in a Paracrine Fashion. Mol Cancer Res *17*, 20-29. 10.1158/1541-7786.MCR-18-0341.
3. Wang, R., Bhattacharya, R., Ye, X., Fan, F., Boulbes, D.R., Xia, L., and Ellis, L.M. (2017). Endothelial cells activate the cancer stem cell-associated NANOGP8 pathway in colorectal cancer cells in a paracrine fashion. Mol Oncol *11*, 1023-1034. 10.1002/1878-0261.12071.
4. Wang, R., Ye, X., Bhattacharya, R., Boulbes, D.R., Fan, F., Xia, L., and Ellis, L.M. (2016). A Disintegrin and Metalloproteinase Domain 17 Regulates Colorectal Cancer Stem Cells and Chemosensitivity Via Notch1 Signaling. Stem Cells Transl Med *5*, 331-338. 10.5966/sctm.2015-0168.
5. Rathore, M., Zhang, W., Wright, M., Zarei, M., Vaziri-Gohar, A., Hajihassani, O., Abbas, A., Feng, H., Brody, J., Markowitz, S.D., et al. (2022). Liver Endothelium Microenvironment Promotes HER3-mediated Cell Growth in Pancreatic Ductal Adenocarcinoma. Journal of cancer science and clinical therapeutics *6*, 431-445. 10.26502/jcsct.5079182.
6. Rathore, M., Zhang, W., Wright, M.I., Bhattacharya, R., Fan, F., Vaziri-Gohar, A., Winter, J., Wang, Z., Markowitz, S.D., Willis, J., et al. (2022). Liver Endothelium Promotes HER3-mediated Cell Survival in Colorectal Cancer with Wild-type and Mutant KRAS. Molecular Cancer Research. 10.1158/1541-7786.Mcr-21-0633.
7. Wang, X., Abraham, S., McKenzie, J.A.G., Jeffs, N., Swire, M., Tripathi, V.B., Luhmann, U.F.O., Lange, C.A.K., Zhai, Z., Arthur, H.M., et al. (2013). LRG1 promotes angiogenesis by modulating endothelial TGF-beta signalling. Nature *499*, 306-311. 10.1038/nature12345.
8. O'Connor, M.N., Kallenberg, D.M., Camilli, C., Pilotti, C., Dritsoula, A., Jackstadt, R., Bowers, C.E., Watson, H.A., Alatsatianos, M., Ohme, J., et al. (2021). LRG1 destabilizes tumor vessels and restricts immunotherapeutic potency. Med (New York, N.Y.) *2*, 1231-1252.e1210. 10.1016/j.medj.2021.10.002.
9. Siegel, R.L., Miller, K.D., Fuchs, H.E., and Jemal, A. (2022). Cancer statistics, 2022. CA Cancer J Clin *72*, 7-33. 10.3322/caac.21708.
10. Siebenhuner, A.R., Guller, U., and Warschkow, R. (2020). Population-based SEER analysis of survival in colorectal cancer patients with or without resection of lung and liver metastases. BMC Cancer *20*, 246. 10.1186/s12885-020-6710-1.
11. Terai, M., Mastrangleo, M., and Sato, T. (2017). Immunological aspect of the liver and metastatic uveal melanoma. J Cancer Metastasis Treat *3*, 231-243. 10.20517/2394-4722.2017.39.
12. Inverso, D., Shi, J., Lee, K.H., Jakab, M., Ben-Moshe, S., Kulkarni, S.R., Schneider, M., Wang, G., Komeili, M., Velez, P.A., et al. (2021). A spatial vascular transcriptomic, proteomic, and phosphoproteomic atlas unveils an angiocrine Tie-Wnt signaling axis in the liver. Dev Cell *56*, 1677-1693 e1610. 10.1016/j.devcel.2021.05.001.
13. Gracia-Sancho, J., Caparros, E., Fernandez-Iglesias, A., and Frances, R. (2021). Role of liver sinusoidal endothelial cells in liver diseases. Nat Rev Gastroenterol Hepatol *18*, 411-431. 10.1038/s41575-020-00411-3.
14. Tokumoto, M.W., Tanaka, H., Tauchi, Y., Kasashima, H., Kurata, K., Yashiro, M., Sakurai, K., Toyokawa, T., Kubo, N., Amano, R., et al. (2015). Identification of tumour-reactive lymphatic endothelial cells capable of inducing progression of gastric cancer. Br J Cancer *113*, 1046-1054. 10.1038/bjc.2015.282.

15. Butler, J.M., Kobayashi, H., and Rafii, S. (2010). Instructive role of the vascular niche in promoting tumour growth and tissue repair by angiocrine factors. Nat Rev Cancer *10*, 138-146. 10.1038/nrc2791.
16. Wang, Y.H., Dong, Y.Y., Wang, W.M., Xie, X.Y., Wang, Z.M., Chen, R.X., Chen, J., Gao, D.M., Cui, J.F., and Ren, Z.G. (2013). Vascular endothelial cells facilitated HCC invasion and metastasis through the Akt and NF-kappaB pathways induced by paracrine cytokines. J Exp Clin Cancer Res *32*, 51. 10.1186/1756-9966-32-51.
17. Alsina-Sanchis, E., Mulfarth, R., and Fischer, A. (2021). Control of Tumor Progression by Angiocrine Factors. Cancers (Basel) *13*. 10.3390/cancers13112610.
18. Haikala, H.M., and Janne, P.A. (2021). Thirty Years of HER3: From Basic Biology to Therapeutic Interventions. Clin Cancer Res *27*, 3528-3539. 10.1158/1078-0432.CCR-20-4465.
19. Sequist, L.V., Gray, J.E., Harb, W.A., Lopez-Chavez, A., Doebele, R.C., Modiano, M.R., Jackman, D.M., Baggstrom, M.Q., Atmaca, A., Felip, E., et al. (2019). Randomized Phase II Trial of Seribantumab in Combination with Erlotinib in Patients with EGFR Wild-Type Non-Small Cell Lung Cancer. Oncologist *24*, 1095-1102. 10.1634/theoncologist.2018-0695.
20. Jonna, S., Feldman, R.A., Swensen, J., Gatalica, Z., Korn, W.M., Borghaei, H., Ma, P.C., Nieva, J.J., Spira, A.I., Vanderwalde, A.M., et al. (2019). Detection of NRG1 Gene Fusions in Solid Tumors. Clin Cancer Res *25*, 4966-4972. 10.1158/1078-0432.Ccr-19-0160.
21. Jones, M.R., Williamson, L.M., Topham, J.T., Lee, M.K.C., Goytain, A., Ho, J., Denroche, R.E., Jang, G., Pleasance, E., Shen, Y., et al. (2019). NRG1 Gene Fusions Are Recurrent, Clinically Actionable Gene Rearrangements in KRAS Wild-Type Pancreatic Ductal Adenocarcinoma. Clin Cancer Res *25*, 4674-4681. 10.1158/1078-0432.CCR-19-0191.
22. Heining, C., Horak, P., Uhrig, S., Codo, P.L., Klink, B., Hutter, B., Frohlich, M., Bonekamp, D., Richter, D., Steiger, K., et al. (2018). NRG1 Fusions in KRAS Wild-Type Pancreatic Cancer. Cancer Discov *8*, 1087-1095. 10.1158/2159-8290.CD-18-0036.
23. Zhao, W., and Lin, J. (2021). [Neuregulin 2 is highly expressed in glioma tissues to regulate glial fibrillary acidic protein expression via Akt signaling]. Nan Fang Yi Ke Da Xue Xue Bao *41*, 1171-1176. 10.12122/j.issn.1673-4254.2021.08.07.
24. Chang, H., Riese, D.J., 2nd, Gilbert, W., Stern, D.F., and McMahan, U.J. (1997). Ligands for ErbB-family receptors encoded by a neuregulin-like gene. Nature *387*, 509-512. 10.1038/387509a0.
25. De Rossi, G., Da Vitoria Lobo, M.E., Greenwood, J., and Moss, S.E. (2022). LRG1 as a novel therapeutic target in eye disease. Eye. 10.1038/s41433-021-01807-4.
26. Camilli, C., Hoeh, A.E., De Rossi, G., Moss, S.E., and Greenwood, J. (2022). LRG1: an emerging player in disease pathogenesis. Journal of Biomedical Science *29*, 6. 10.1186/s12929-022-00790-6.
27. Markowitz, S., Wang, J., Myeroff, L., Parsons, R., Sun, L., Lutterbaugh, J., Fan, R.S., Zborowska, E., Kinzler, K.W., Vogelstein, B., and et al. (1995). Inactivation of the type II TGF-beta receptor in colon cancer cells with microsatellite instability. Science *268*, 1336-1338. 10.1126/science.7761852.
28. Liu, S., Ren, J., and ten Dijke, P. (2021). Targeting TGFβ signal transduction for cancer therapy. Signal Transduction and Targeted Therapy *6*, 8. 10.1038/s41392-020-00436-9.
29. Kallenberg, D., Tripathi, V., Javaid, F., Pilotti, C., George, J., Davis, S., Blackburn, J.W., O'Connor, M., Dowsett, L., Bowers, C.E., et al. (2021). A Humanized Antibody against LRG1 that Inhibits Angiogenesis and Reduces Retinal Vascular Leakage. bioRxiv, 2020.2007.2025.218149. 10.1101/2020.07.25.218149.
30. Singhal, M., Gengenbacher, N., Abdul Pari, A.A., Kamiyama, M., Hai, L., Kuhn, B.J., Kallenberg, D.M., Kulkarni, S.R., Camilli, C., Preuß, S.F., et al. (2021). Temporal multi-omics identifies LRG1 as

a vascular niche instructor of metastasis. Sci Transl Med *13*, eabe6805. 10.1126/scitranslmed.abe6805.

31. O'Connor, M.N., Kallenberg, D.M., Camilli, C., Pilotti, C., Dritsoula, A., Jackstadt, R., Bowers, C.E., Watson, H.A., Alatsatianos, M., Ohme, J., et al. (2021). LRG1 destabilizes tumor vessels and restricts immunotherapeutic potency. Med *2*, 1231-1252.e1210. https://doi.org/10.1016/j.medj.2021.10.002.
32. Batool, A., Aashaq, S., and Andrabi, K.I. (2019). Eukaryotic initiation factor 4E (eIF4E): A recap of the cap-binding protein. J Cell Biochem *120*, 14201-14212. 10.1002/jcb.28851.
33. Shahbazian, D., Roux, P.P., Mieulet, V., Cohen, M.S., Raught, B., Taunton, J., Hershey, J.W., Blenis, J., Pende, M., and Sonenberg, N. (2006). The mTOR/PI3K and MAPK pathways converge on eIF4B to control its phosphorylation and activity. The EMBO Journal *25*, 2781-2791. https://doi.org/10.1038/sj.emboj.7601166.
34. Hao, P., Yu, J., Ward, R., Liu, Y., Hao, Q., An, S., and Xu, T. (2020). Eukaryotic translation initiation factors as promising targets in cancer therapy. Cell Communication and Signaling *18*, 175. 10.1186/s12964-020-00607-9.
35. Hao, Y., Samuels, Y., Li, Q., Krokowski, D., Guan, B.-J., Wang, C., Jin, Z., Dong, B., Cao, B., Feng, X., et al. (2016). Oncogenic PIK3CA mutations reprogram glutamine metabolism in colorectal cancer. Nature Communications *7*, 11971. 10.1038/ncomms11971.
36. Creson, T.K., Yuan, P., Manji, H.K., and Chen, G. (2009). Evidence for involvement of ERK, PI3K, and RSK in induction of Bcl-2 by valproate. Journal of molecular neuroscience : MN *37*, 123-134. 10.1007/s12031-008-9122-2.
37. Hao, Y., Wang, C., Cao, B., Hirsch, B.M., Song, J., Markowitz, S.D., Ewing, R.M., Sedwick, D., Liu, L., Zheng, W., and Wang, Z. (2013). Gain of interaction with IRS1 by p110α-helical domain mutants is crucial for their oncogenic functions. Cancer Cell *23*, 583-593. 10.1016/j.ccr.2013.03.021.
38. Hao, Y., Samuels, Y., Li, Q., Krokowski, D., Guan, B.J., Wang, C., Jin, Z., Dong, B., Cao, B., Feng, X., et al. (2016). Oncogenic PIK3CA mutations reprogram glutamine metabolism in colorectal cancer. Nat Commun *7*, 11971. 10.1038/ncomms11971.
39. Ladd, J.J., Busald, T., Johnson, M.M., Zhang, Q., Pitteri, S.J., Wang, H., Brenner, D.E., Lampe, P.D., Kucherlapati, R., Feng, Z., et al. (2012). Increased plasma levels of the APC-interacting protein MAPRE1, LRG1, and IGFBP2 preceding a diagnosis of colorectal cancer in women. Cancer Prev Res (Phila) *5*, 655-664. 10.1158/1940-6207.CAPR-11-0412.
40. Zhou, Y., Zhang, X., Zhang, J., Fang, J., Ge, Z., and Li, X. (2017). LRG1 promotes proliferation and inhibits apoptosis in colorectal cancer cells via RUNX1 activation. PLoS One *12*, e0175122. 10.1371/journal.pone.0175122.
41. Zhang, J., Zhu, L., Fang, J., Ge, Z., and Li, X. (2016). LRG1 modulates epithelial-mesenchymal transition and angiogenesis in colorectal cancer via HIF-1alpha activation. J Exp Clin Cancer Res *35*, 29. 10.1186/s13046-016-0306-2.
42. Zhang, J., Zhu, L., Fang, J., Ge, Z., and Li, X. (2016). LRG1 modulates epithelial-mesenchymal transition and angiogenesis in colorectal cancer via HIF-1α activation. Journal of Experimental & Clinical Cancer Research *35*, 29. 10.1186/s13046-016-0306-2.

Figure 1

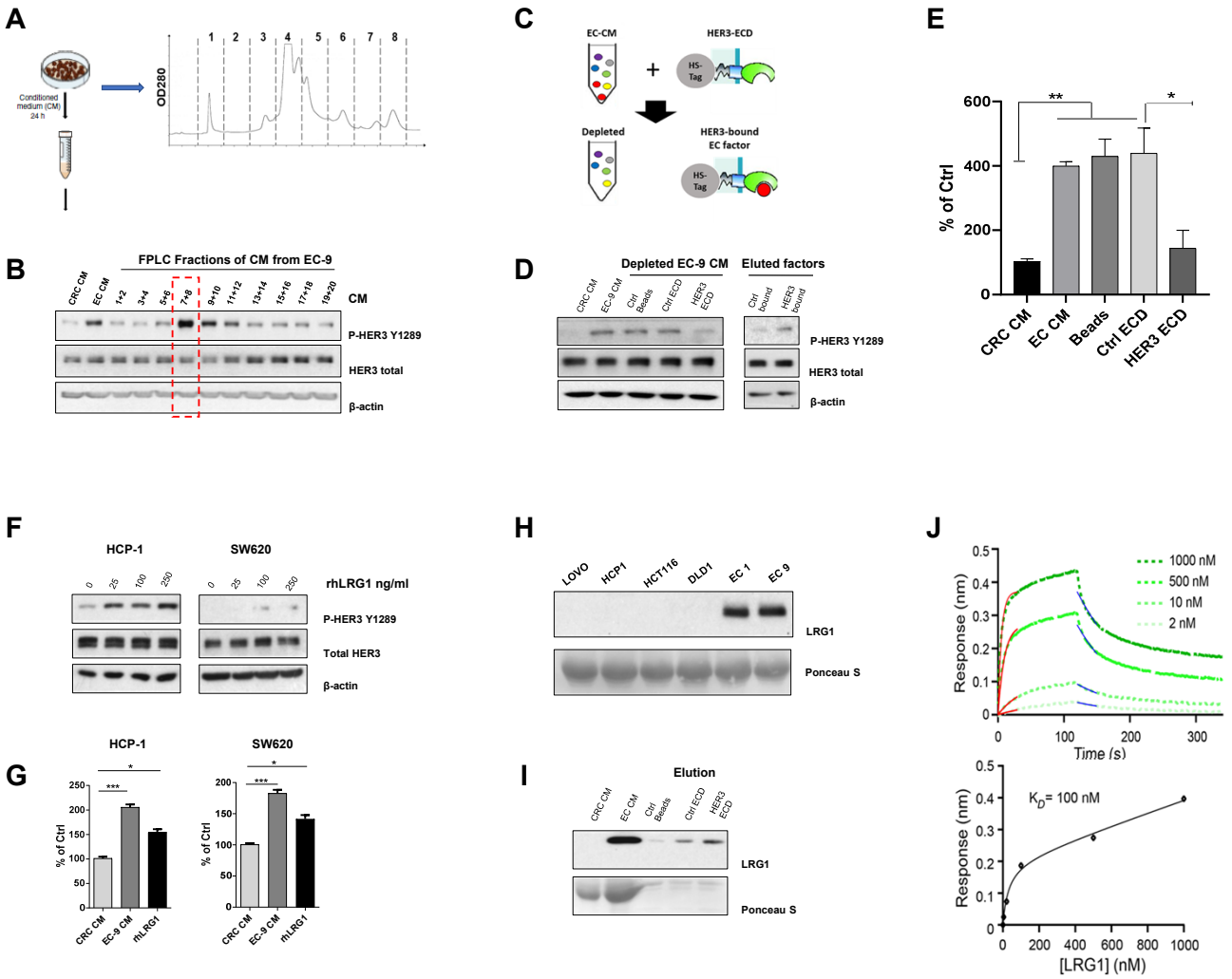
A
Conditioned medium (CM) 24 h
OD280
1 2 3 4 5 6 7 8
B
FPLC Fractions of CM from EC-9
CRC CM
EC CM
1+2
3+4
5+6
7+8
9+10
11+12
13+14
15+16
17+18
19+20
CM
P-HER3 Y1289
HER3 total
β-actin
C
EC-CM
HER3-ECD
HS-Tag
Depleted
HER3-bound EC factor
D
Depleted EC-9 CM
Eluted factors
CRC CM
EC-9 CM
Ctrl Beads
Ctrl ECD
HER3 ECD
Ctrl bound
HER3 bound
P-HER3 Y1289
HER3 total
β-actin
E
% of Ctrl
600
400
200
0
**
*
CRC CM
EC CM
Beads
Ctrl ECD
HER3 ECD
F
HCP-1
SW620
0
25
100
250
rhLRG1 ng/ml
P-HER3 Y1289
Total HER3
β-actin
G
HCP-1
SW620
% of Ctrl
***
*
CRC CM
EC-9 CM
rhLRG1
H
LOVO
HCP1
HCT116
DLD1
EC 1
EC 9
LRG1
Ponceau S
I
Elution
CRC CM
EC CM
Ctrl Beads
Ctrl ECD
HER3 ECD
LRG1
Ponceau S
J
1000 nM
500 nM
10 nM
2 nM
Response (nm)
Time (s)
0
100
200
300
0.5
0.4
0.3
0.2
0.1
0
K_D= 100 nM
[LRG1] (nM)
0
200
400
600
800
1000

Figure 2

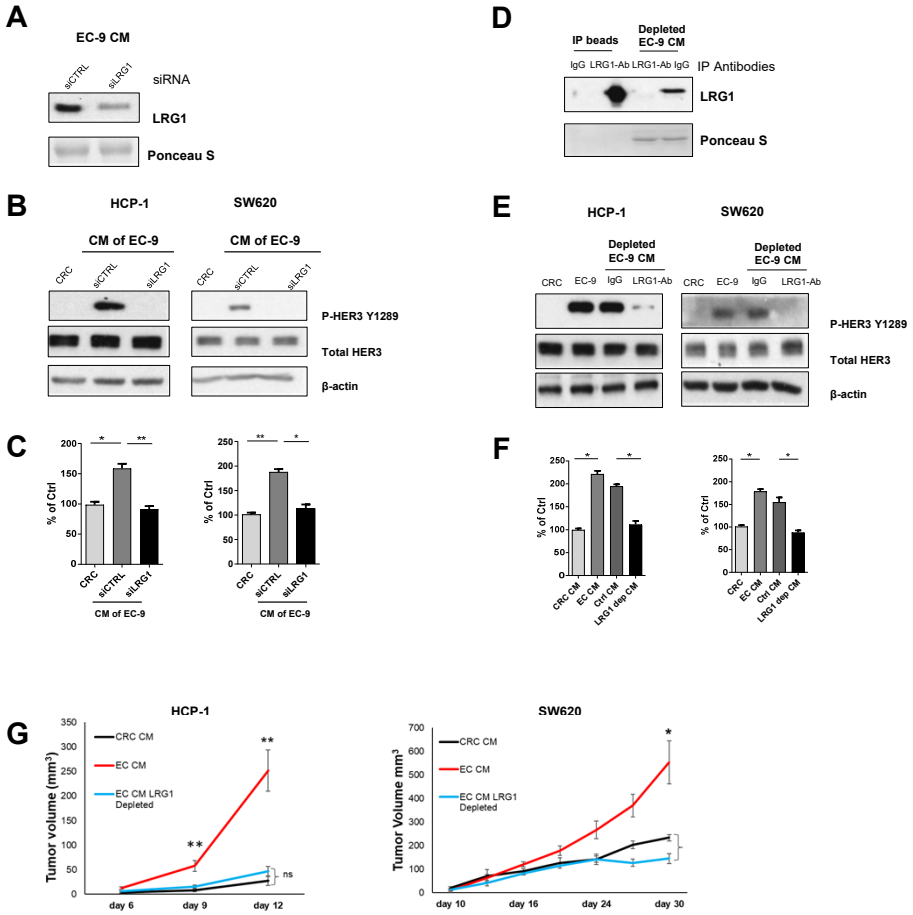
A
EC-9 CM
siCTRL
siLRG1
siRNA
LRG1
Ponceau S
D
IP beads
Depleted EC-9 CM
IgG LRG1-Ab LRG1-Ab IgG
IP Antibodies
LRG1
Ponceau S
B
HCP-1
SW620
CM of EC-9
CM of EC-9
CRC
siCTRL
siLRG1
P-HER3 Y1289
Total HER3
β-actin
E
HCP-1
SW620
Depleted EC-9 CM
Depleted EC-9 CM
CRC EC-9 IgG LRG1-Ab
CRC EC-9 IgG LRG1-Ab
P-HER3 Y1289
Total HER3
β-actin
C
% of Ctrl
CRC
siCTRL
siLRG1
CM of EC-9
F
% of Ctrl
CRC CM
EC CM
Ctrl CM
LRG1 dep CM
G
HCP-1
Tumor volume (mm³)
CRC CM
EC CM
EC CM LRG1 Depleted
ns
day 6
day 9
day 12
SW620
Tumor Volume mm³
CRC CM
EC CM
EC CM LRG1 Depleted
day 10
day 16
day 24
day 30

Figure 3

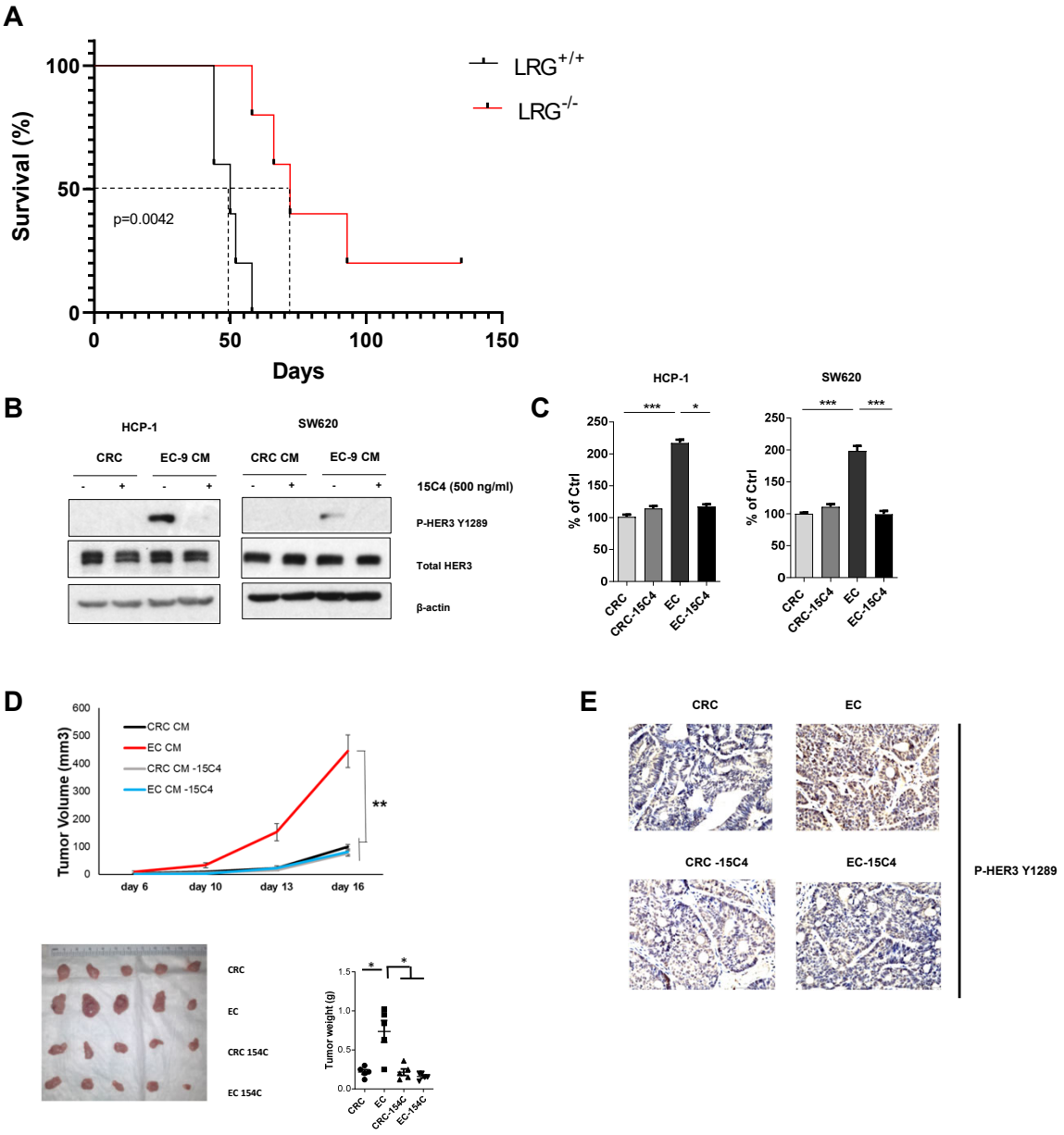
A
Survival (%)
100
50
0
p=0.0042
0
50
100
150
Days
LRG+/+
LRG-/-
B
HCP-1
SW620
CRC
EC-9 CM
CRC CM
EC-9 CM
15C4 (500 ng/ml)
P-HER3 Y1289
Total HER3
β-actin
C
HCP-1
SW620
% of Ctrl
CRC
CRC-15C4
EC
EC-15C4
D
Tumor Volume (mm3)
CRC CM
EC CM
CRC CM -15C4
EC CM -15C4
day 6
day 10
day 13
day 16
CRC
EC
CRC 154C
EC 154C
Tumor weight (g)
E
CRC
EC
CRC -15C4
EC-15C4
P-HER3 Y1289

Figure 4

A

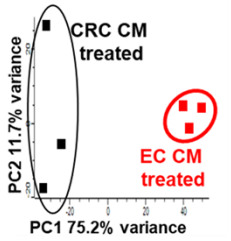

B

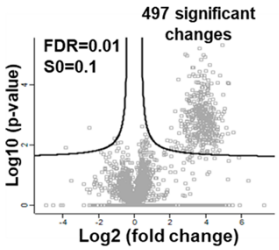

Table 2. Summary of top activated pathways

Top Cellular Functions	p-value range
Protein Synthesis	1.05E-05-3.47E-17
Cell death & Survival	1.15E-03-4.21E-11
Gene Expression	1.11E-03-7.23E-11
Top Pathways	**p-value**
eIF4 signaling	5.39E-06
mTOR	1.18E-05
ErbB	1.5E-02

C

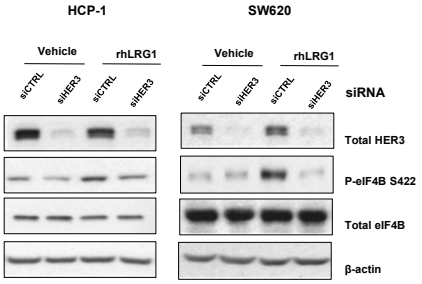

D

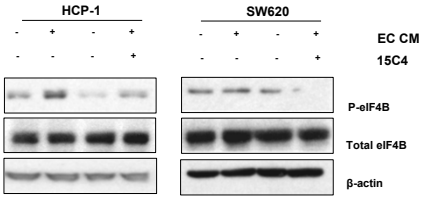

E

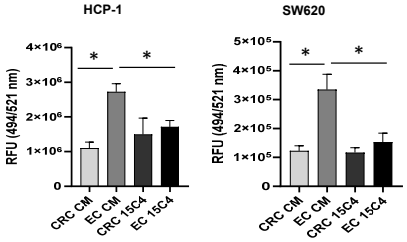

F

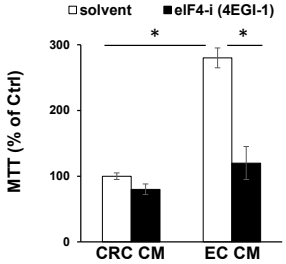

G

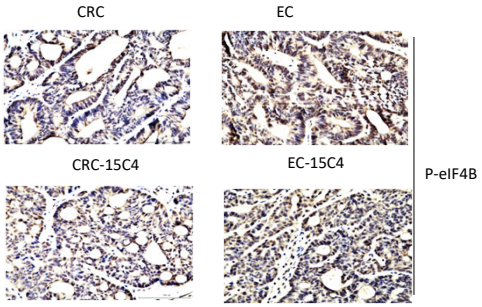

Figure 5

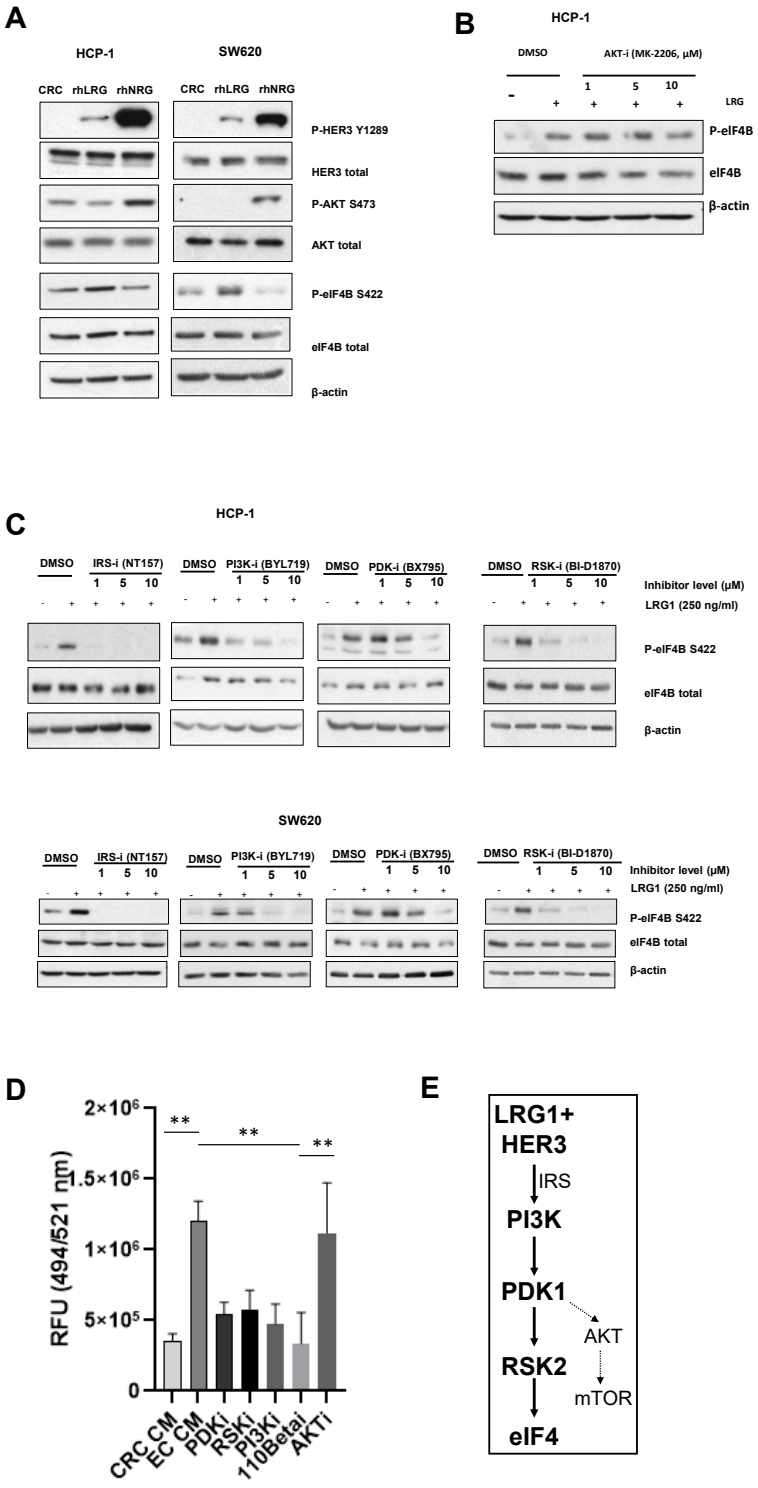
A
HCP-1
SW620
CRC rhLRG rhNRG
P-HER3 Y1289
HER3 total
P-AKT S473
AKT total
P-eIF4B S422
eIF4B total
β-actin
B
HCP-1
DMSO
AKT-i (MK-2206, μM)
1 5 10
LRG
P-eIF4B
eIF4B
β-actin
C
HCP-1
DMSO
IRS-i (NT157)
PI3K-i (BYL719)
PDK-i (BX795)
RSK-i (BI-D1870)
1 5 10
Inhibitor level (μM)
LRG1 (250 ng/ml)
P-eIF4B S422
eIF4B total
β-actin
SW620
D
RFU (494/521 nm)
2×10^6
1.5×10^6
1×10^6
5×10^5
0
**
CRC CM
EC CM
PDKi
RSKi
PI3Ki
110Betai
AKTi
E
LRG1+
HER3
IRS
PI3K
PDK1
AKT
RSK2
mTOR
eIF4

Supplementary Figure 1

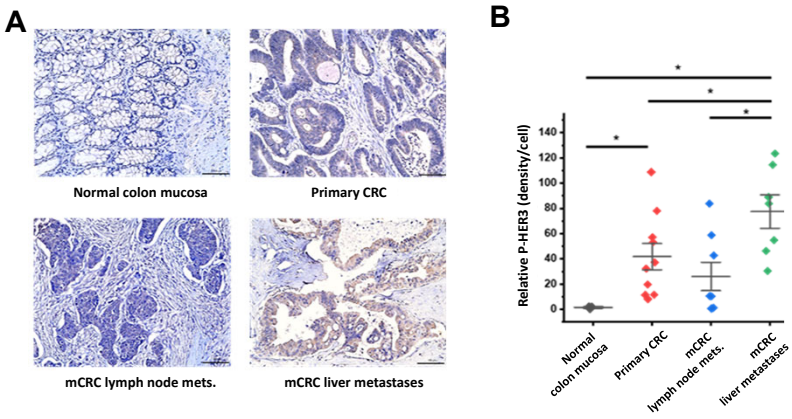

Supplementary Figure 2

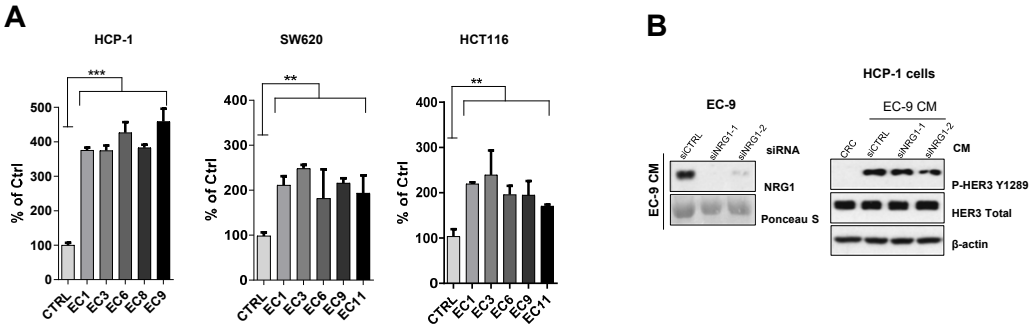

Supplementary Figure 3

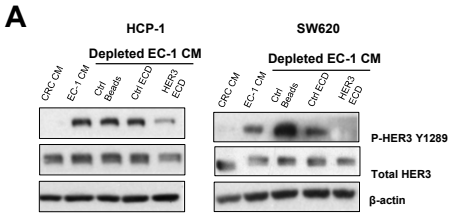

Table 1. Candidate soluble proteins bout to HER3-ECD

Soluble Factor	Molecular Weight
LRG1	45
LTBP3	139
TGFB1	44
IGFBP4	35
NRP1	103
NUCB1	54
EFEMP1	55
FSTL1	35
INHBA	47
DKK3	39

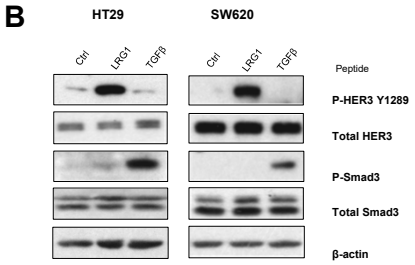
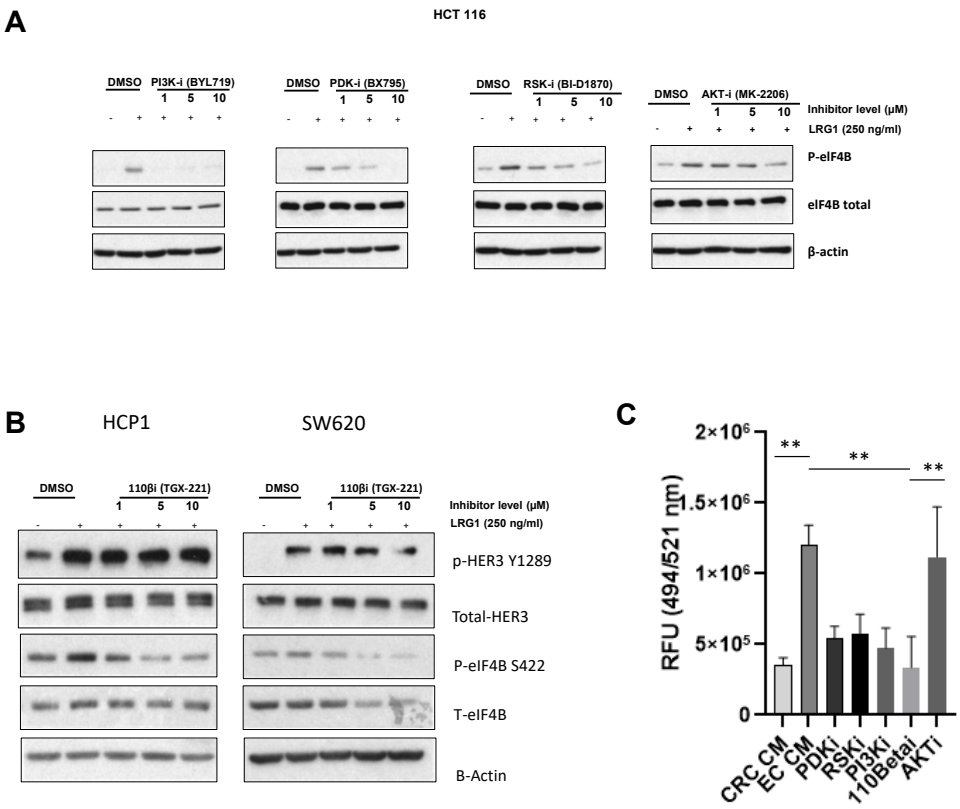
Supplementary Figure 4